Int J Adv Manuf Technol (2007) 35:255–267
DOI 10.1007/s00170-006-0720-2

ORIGINAL ARTICLE

Finite element modeling the influence of edge roundness on the stress and temperature fields induced by high-speed machining

Tuğrul Özel · Erol Zeren

Received: 28 March 2006 / Accepted: 7 July 2006 / Published online: 6 October 2006

Abstract High-speed machining (HSM) may produce parts at high production rates with substantially higher fatigue strengths and increased subsurface micro-hardness and plastic deformation, mostly due to the ploughing of the round cutting tool edge associated with induced stresses, and can have far more superior surface properties than surfaces generated by grinding and polishing. Cutting edge roundness may induce stress and temperature fields on the machined subsurface and influence the finished surface properties, as well as tool life. In this paper, a finite element method (FEM) modeling approach with arbitrary Lagrangian Eulerian (ALE) fully coupled thermal-stress analysis is employed. In order to realistically simulate HSM using edge design tools, an FEM model for orthogonal cutting is designed, and solution techniques such as adaptive meshing and explicit dynamics are performed. A detailed friction modeling at the tool–chip and tool–work interfaces is also carried out. Work material flow around the round edge cutting tool is successfully simulated without implementing a chip separation criterion and without the use of a remeshing scheme. The FEM modeling of the stresses and the resultant surface properties induced by round edge cutting tools is performed for the HSM of AISI 4340 steel. Once FEM simulations are complete for different edge radii and depths of cut, the tool is unloaded and the stresses are relieved. Predicted stress fields are compared with experimentally measured residual stresses obtained from the literature. The results indicate that the round edge design tools influence the stress and temperature fields greatly. An optimization scheme can be developed to identify the most desirable edge design by using the finite element analysis (FEA) scheme presented in this work.

Keywords Finite element modeling · Edge roundness · Arbitrary Lagrangian Eulerian method · Machining-induced stresses

T. Özel (✉) · E. Zeren
Department of Industrial and Systems Engineering,
Rutgers University,
Piscataway, NJ 08854, USA
e-mail: ozel@rci.rutgers.edu

1 Introduction

Predicting the physical process and temperature and stress fields accurately play a pivotal role for predictive process engineering for high-speed machining (HSM) processes. Tool edge geometry is particularly important because its influence on obtaining the most desirable tool life and surface integrity is considered to be significant. Finite element method (FEM) modelling based simulation of machining processes has been providing a better understanding of chip formation mechanisms, heat generation in cutting zones, and the resulting stress and temperature fields. Advanced process simulation techniques are essential in order to study the influence of the tool edge geometry and cutting conditions on the surface integrity, especially on the machining-induced stresses. In this paper, an advanced FEM simulation technique is utilized to investigate the physical cutting process for predicting the temperature and stress fields on the machined surface.

As commonly known, there are two types of analysis in which a continuous medium can be described, i.e., Eulerian and Lagrangian, in the FEM modeling of deformation processes. In a Lagrangian analysis, the computational grid deforms with the material, whereas in an Eulerian analysis, it is fixed in space. The Lagrangian calculation embeds a computational mesh in the material domain and solves for

the position of the mesh at discrete points in time. In those analyses, two distinct methods, the implicit and the explicit time integration techniques, can be utilized. The implicit technique is more applicable to solving linear static problems, while the explicit method is more suitable for non-linear dynamic problems.

A majority of earlier numerical models have relied on the Lagrangian formulation [1–6], whereas some of the models utilized the Eulerian formulation [7]. However, it was evident that the Lagrangian formulation required a criterion for the separation of the undeformed chip from the workpiece. For this purpose, several chip separation criteria, such as the strain energy density and the effective strain criteria, were implemented as exclusively reported in [8]. Updated Lagrangian implicit formulation with automatic remeshing without using chip separation criteria has also been used in the simulation of continuous and segmented chip formation in machining processes [9–16].

The arbitrary Lagrangian Eulerian (ALE) technique combines the features of pure Lagrangian analysis and Eulerian analysis. ALE formulation is also utilized in simulating machining to avoid frequent remeshing for chip separation [17–23]. Explicit dynamic ALE formulation is very efficient for simulating highly non-linear problems involving large localized deformations and changing contact conditions, such as those experienced in machining. The explicit dynamic procedure performs a large number of small time increments efficiently. The adaptive meshing technique does not alter the elements or connectivity of the mesh. This technique allows free boundary conditions whereby only a small part of the workpiece in the vicinity of the tool tip needs to be modeled.

On the other hand, the friction in metal cutting plays an important role in the thermo-mechanical chip flow and integrity of the machined work surface. The most common approach in modeling the friction at the chip–tool interface is to use an average coefficient of friction. Late models consist of a sticking region for which the friction force is constant, and a sliding region for which the friction force varies linearly according to Coulomb's law.

FEM simulation of machining using edge design tools is essential in order to predict realistic stress and temperature fields occurring in HSM. Recent FEM studies reported in the literature include the effects of edge geometries in the orthogonal cutting process [24, 25], simulation of machining non-homogenous materials [26], and predicting stresses on the machined surfaces of hardened steels [27–29]. Recently, Guo and Wen [30] used FEM simulations to investigate the effects of stagnation and round edge geometry on chip morphology and stress and temperature fields on the machined surface. Davies et al. [31] investigated the effects of work material models on the predictions of the FEM simulations. Deshayes et al. [32] simulated the serrated chip formation in orthogonal machining and presented comparisons with experimental results.

The round edge of the cutting tool and the highly deformed region underneath has a dominant influence on the residual stresses of the machined surface. This also signifies the proposed work when compared with the earlier FEM modeling studies that relied on chip–workpiece separation criteria. The use of a separation criterion undermines the effect of the cutting edge on the residual stress formation on the machined surface.

In this paper, ALE formulation with pure Lagrangian boundaries is applied in the simulation of machining with round edge cutting tools and by utilizing an adaptive meshing technique. The work material is allowed to flow around the round edge of the cutting tool so that the physical process can be simulated more realistically.

2 Orthogonal machining of AISI 4340 steel

In this study, the finite element analysis (FEA) of machining-induced temperature and stress fields in the orthogonal cutting of AISI 4340 steel with round carbide edge cutting tools are investigated. An experimental study conducted by Jacobus et al. [33], where the orthogonal cutting of tubes was performed, is utilized in order to validate the predicted machining-induced residual stresses. In their experimental design, Jacobus et al. [33] varied the tool edge roundness, uncut chip thickness (depth of cut), and used a constant cutting speed of 300 m/min, as shown in Table 1. The uncoated tungsten carbide tool with the tool holder provided a 3° rake angle and an 8° clearance angle. All of the cutting conditions revealed orthogonal machining with continuous chip formation [33].

2.1 Work material constitutive modeling

In FEA, accurate flow stress models are considered to be highly necessary to represent work material constitutive behavior under high-strain-rate deformation conditions. The constitutive model proposed by Johnson and Cook [34] describes the flow stress of a material with the product of

Table 1 Cutting conditions

Test no.	Uncut chip thickness (mm)	Edge radius (mm)	Cutting speed (m/min)
1	0.10	0.025	300
2	0.10	0.075	300
3	0.20	0.025	300
4	0.20	0.075	300

Table 2 Constants of the Johnson-Cook (J-C) constitutive model for the work materials [35]

Material	*A* (MPa)	*B* (MPa)	*n*	*C*	*m*	T_{melt} (°C)
AISI 4340 steel	792.0	510.0	0.26	0.014	1.03	1,520

strain, strain rate, and temperature effects that are individually determined as given in Eq. 1:

$$\overline{\sigma} = [\mathrm{A} + \mathrm{B}(\overline{\varepsilon})^{\mathrm{n}}]\left[1 + \mathrm{C}\, ln\left(\frac{\dot{\overline{\varepsilon}}}{\dot{\overline{\varepsilon}}_0}\right)\right]\left[1 - \left(\frac{\mathrm{T} - \mathrm{T}_{\mathrm{room}}}{\mathrm{T}_{\mathrm{melt}} - \mathrm{T}_{\mathrm{room}}}\right)^{\mathrm{m}}\right] \tag{1}$$

In the Johnson-Cook (J-C) model, the constant *A* is, in fact, the initial yield strength of the material at room temperature and a strain rate of 1/*s* and $\overline{\varepsilon}$ represents the plastic equivalent strain. The strain rate $\dot{\overline{\varepsilon}}$ is normalized with a reference strain rate $\dot{\overline{\varepsilon}}_0$ Temperature term in the J-C model reduces the flow stress to zero at the melting temperature of the work material, leaving the constitutive model with no temperature effect. In this study, the FEA of the machining of AISI 4340 steel in annealed condition is investigated and its J-C material model constants are given in Table 2.

2.2 Variable friction modeling

As commonly accepted, along the tool–chip contact area near the cutting edge, a sticking region forms, and the frictional shearing stress at the sticking region, τ_p, becomes equal to the average shear flow stress at the tool–chip interface on the chip, k_{chip}, $\tau_p = k_{\mathrm{chip}}$ [13]. Over the remainder of the tool–chip contact area, a sliding region forms, and the frictional shearing stress can be determined by using a coefficient of friction, μ, (see Fig. 1).

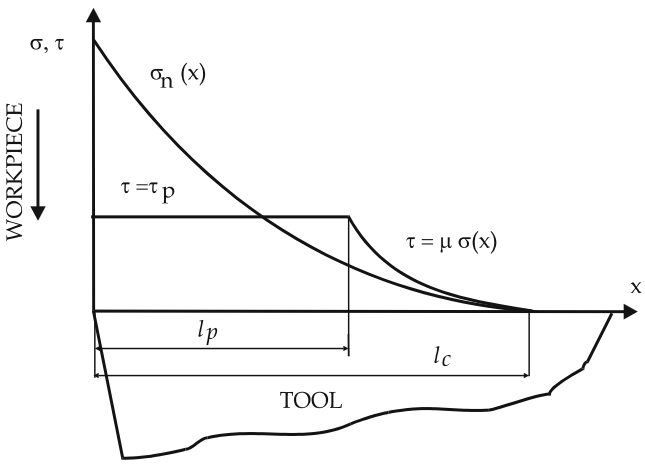

Fig. 1 Normal and frictional stress distributions on the tool rake face [13]

When the normal stress distribution over the rake face is fully defined and the coefficient of friction, μ, is known, the frictional stress can be determined. The shear stress distribution on the tool rake face can be represented as two distinct regions:

– (1) In the sticking region:

$$\tau_{\mathrm{f}}(\mathrm{x}) = \tau_{\mathrm{p}} = \mathrm{k}_{\mathrm{chip}} \text{ and when } \mu\sigma_{\mathrm{n}}(\mathrm{x}) \geq \tau_{\mathrm{p}}, \quad 0 < \mathrm{x} \leq l_{\mathrm{p}} \tag{2a}$$

– (2) In the sliding region:

$$\tau_{\mathrm{f}}(\mathrm{x}) = \mu\sigma_{\mathrm{n}}(\mathrm{x}) \text{ and when } \mu\sigma_{\mathrm{n}}(\mathrm{x}) < \tau_{\mathrm{p}}, \quad l_{\mathrm{p}} < \mathrm{x} \leq l_{\mathrm{c}} \tag{2b}$$

The friction characteristics that are calculated with the methodology explained in Özel and Zeren [36] include parameters of the normal and frictional stress distributions on the tool rake face. Since the length of the sticking region, l_p, and the chip–tool contact length, l_c, are not implemented in the friction model in the FEM simulations, they are not given in Table 3. Instead, a limiting shear friction model is implemented with the limiting shear stress and friction coefficients that are given in Table 3.

3 Finite element modeling

The essential and desired attributes of continuum-based FEM models for cutting are: (1) the work material model should satisfactorily represent elastic, plastic, and thermo-mechanical behavior of the work material deformations observed during the machining process; (2) the FEM model should not require chip separation criteria that highly deteriorate the physical process simulation around the tool cutting edge, especially in the presence of a dominant tool edge geometry, such as a round edge and/or a chamfered edge design; (3) interfacial friction characteristics on the tool–chip and tool–work contacts should be modeled highly accurately in order to account for additional heat generation and stress developments due to friction.

Table 3 Properties of the work and tool materials

Properties	AISI 4340 steel	Carbide tool
Expansion (μm/m°C)	1.23	4.7
Density (g/cm^3)	7.85	15.0
Poisson's ratio	0.22	0.20
Specific heat (J/kg/°C)	477	203
Conductivity (W/m°C)	44.5	46.0
Young's modulus (GPa)	208	800

Table 4 Friction characteristics when using an uncoated carbide-cutting tool

	AISI 4340 steel
k_{chip}	250 Mpa when $\mu\sigma_n(x)\tau_p,\ 0 < x \leq l_p$
μ	0.5 when $\mu\sigma_n(x) < \tau_p,\ l_p < x \leq l_p$

In this paper, a commercial software code, ABAQUS/Explicit v6.4, and an explicit dynamic ALE modeling approach is used to conduct the FEM simulation of orthogonal cutting considering round tool edge geometry and all of the above attributes are successfully implemented in the model. The chip formation process is simulated via adaptive meshing and the plastic flow of work material in the vicinity of the round edge of the tool. Therefore, there is no need for a chip separation criterion in the proposed FEM model.

A thermo-mechanical FEM simulation scheme is created by including tool and workpiece thermal and mechanical properties as summarized in Table 4. Both the workpiece and tool models use four-node bilinear displacement and temperature (CPE4RT) quadrilateral elements and a plane-strain assumption for the deformations occurring during the high-speed orthogonal cutting process.

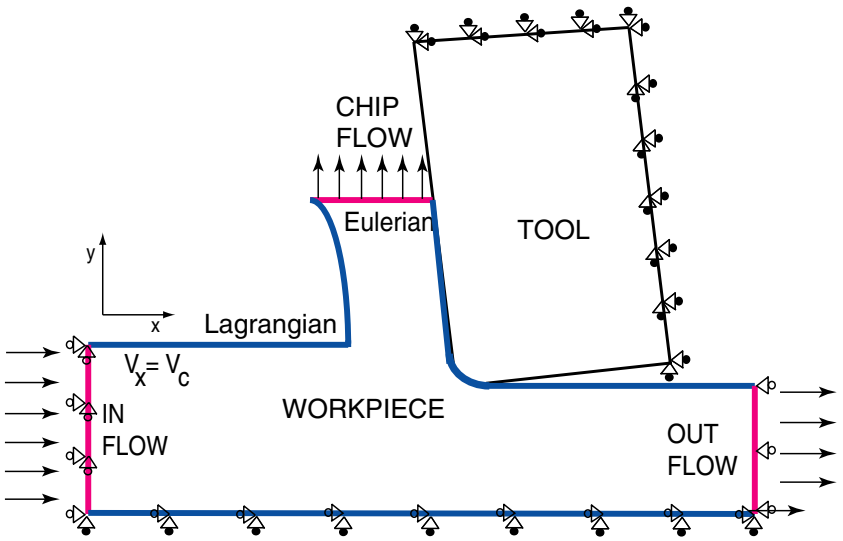

(a)

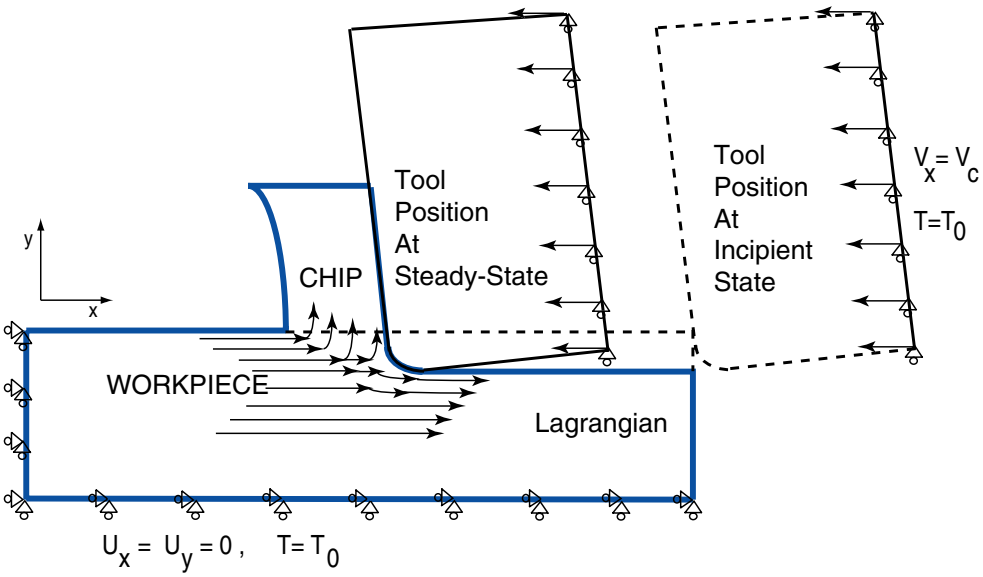

(b)

Fig. 2 Finite element simulation model for ALE formulation with: **a** Eulerian and Lagrangian boundary conditions [37], and **b** pure Lagrangian boundary conditions [23]

3.1 Arbirtrary Lagrangian Eulerian scheme with Eulerian and Lagrangian boundaries

Initially, an ALE model has been designed in which the workpiece is also modeled with the Eulerian boundaries from the inflow, chip flow, and outflow ends, and with the Lagrangian boundaries at the top and the bottom surfaces of the workpiece, as shown in Fig. 2a, as explained by the authors of [37]. The top surface of the workpiece with the free boundaries reaches the final deformed shape at the steady-state cutting and it is allowed to deform without restraint.

In this ALE approach, the general governing equations are solved for both Lagrangian boundaries and Eulerian boundaries in the same fashion. This technique exclusively combines the features of pure Lagrangian analysis and Eulerian analysis, in which the mesh is fixed spatially and the material flows through the mesh, as explained earlier. However, this FEM model requires a pre-defined chip geometry. The chip surfaces are defined with the Lagrangian boundary conditions and the chip upper surface is defined with the Eulerian boundary conditions. Therefore, the chip flow is bound at a vertical position. However, the chip thickness and the chip–tool contact length gradually settle to their final sizes with the change in the deformation conditions as the cutting reaches its steady state.

The major drawback of this ALE approach is that the pre-defined chip shape must be determined beforehand and entered into the FEM model. Similar ALE models were presented by Adibi-Sedeh and Mahdavan [21], Haglund et al. [22], and Özel and Zeren [37].

3.2 Arbirtrary Lagrangian Eulerian scheme with pure Lagrangian boundaries

An FEM simulation model with ALE scheme with pure Lagrangian boundaries is designed and kinematic penalty

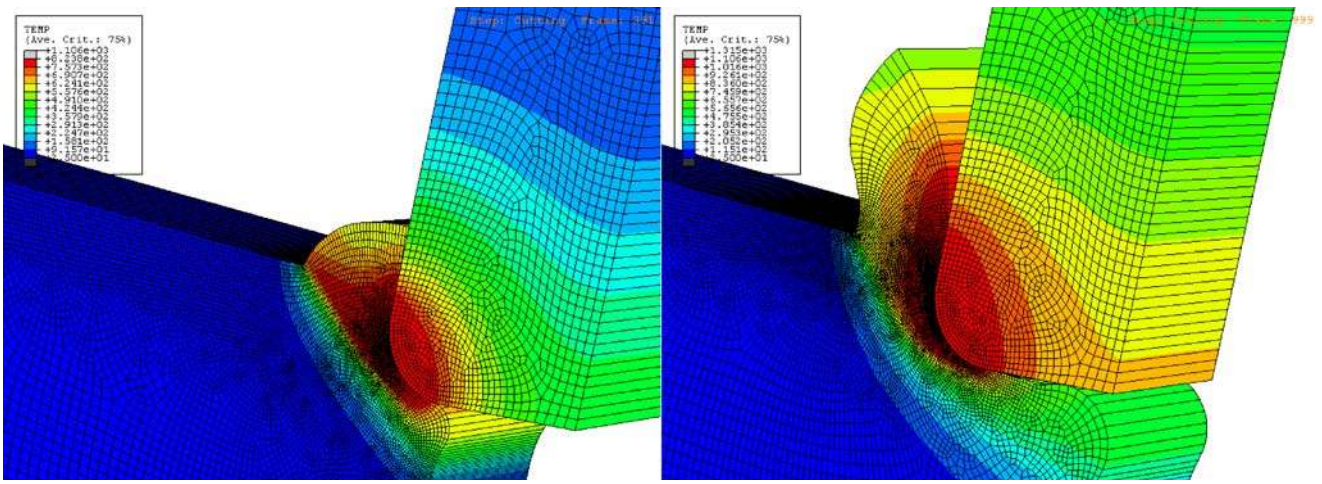

Fig. 3 FEM simulation results using the ALE scheme for machining AISI 4340 steel (test 2)

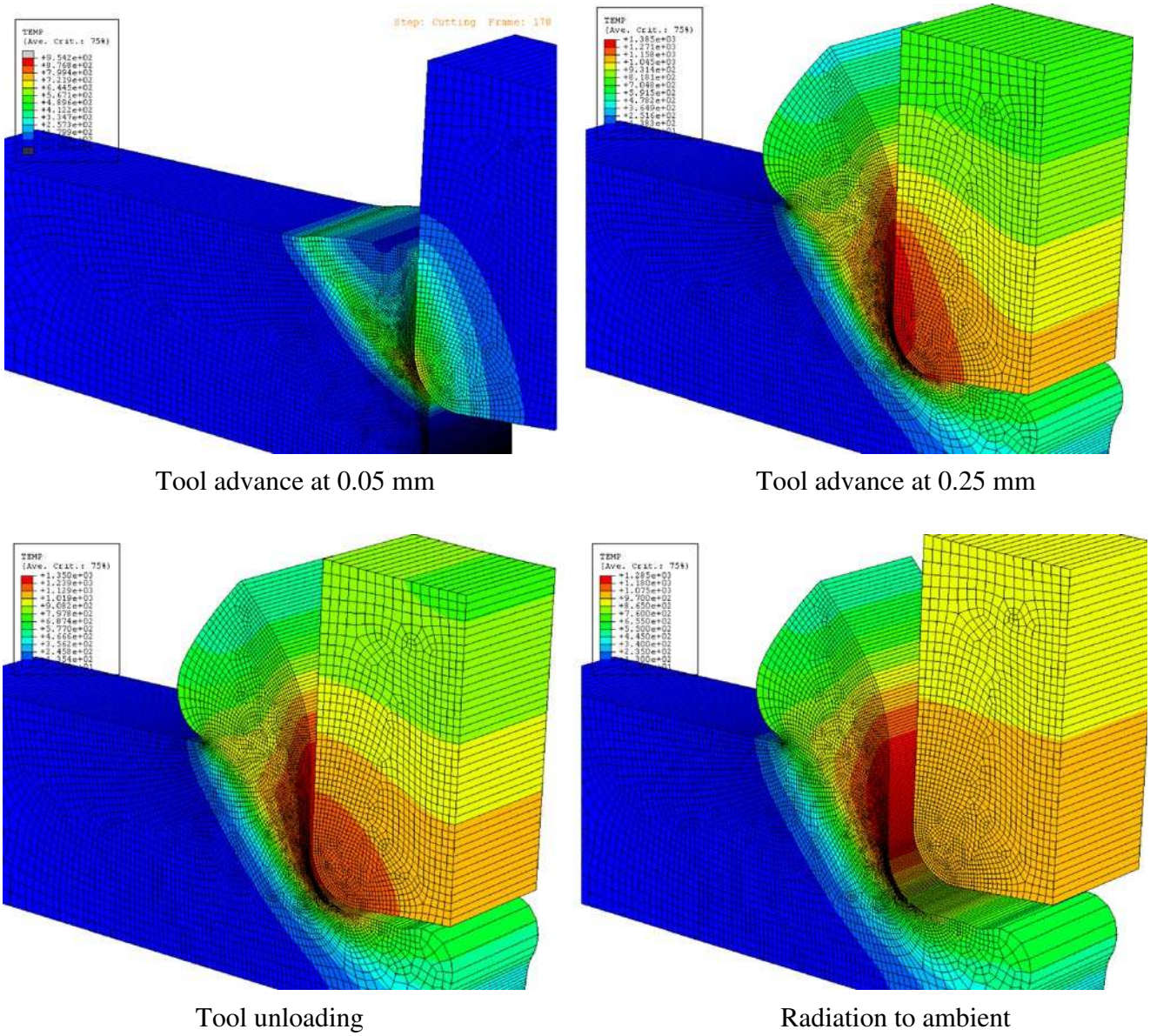

Fig. 4 FEM simulation results using the ALE scheme for machining AISI 4340 steel (test 4)

contact conditions between the tool and the workpiece are defined as shown in Fig. 2b. This model allows an FEM simulation scheme to simulate the chip formation from the incipient to steady state, as proposed by the authors of [23]. In this FEM scheme, the explicit dynamic procedure performs a large number of small time increments efficiently. The adaptive meshing technique does not alter the elements and connectivity of the mesh. This technique combines the features of pure Lagrangian analysis, in which the mesh follows the material, and Eulerian analysis, when it is needed as part of the adaptive meshing, in which the mesh is fixed spatially and the material flows through the mesh. The cutting process as a dynamic event causes large deformations in several numbers of increments, resulting in massive mesh distortion and termination of the FEM simulation. It is highly critical to use adaptive meshing with fine-tuned parameters in order to simulate the plastic flow over the round edge of the tool. Therefore, the intensity, frequency, and sweeping of the adaptive meshing are adjusted to the most optimum setting for maintaining a successful mesh during the simulation of the orthogonal cutting process.

The general equations of motion in explicit dynamic analysis are integrated by using the explicit central difference integration rule with diagonal element mass matrices. The system equations become uncoupled so that each equation can be solved for explicitly. This makes the explicit dynamic method highly efficient for non-linear dynamic problems, such as metal cutting. During metal cutting, the flow stress is highly dependent on the

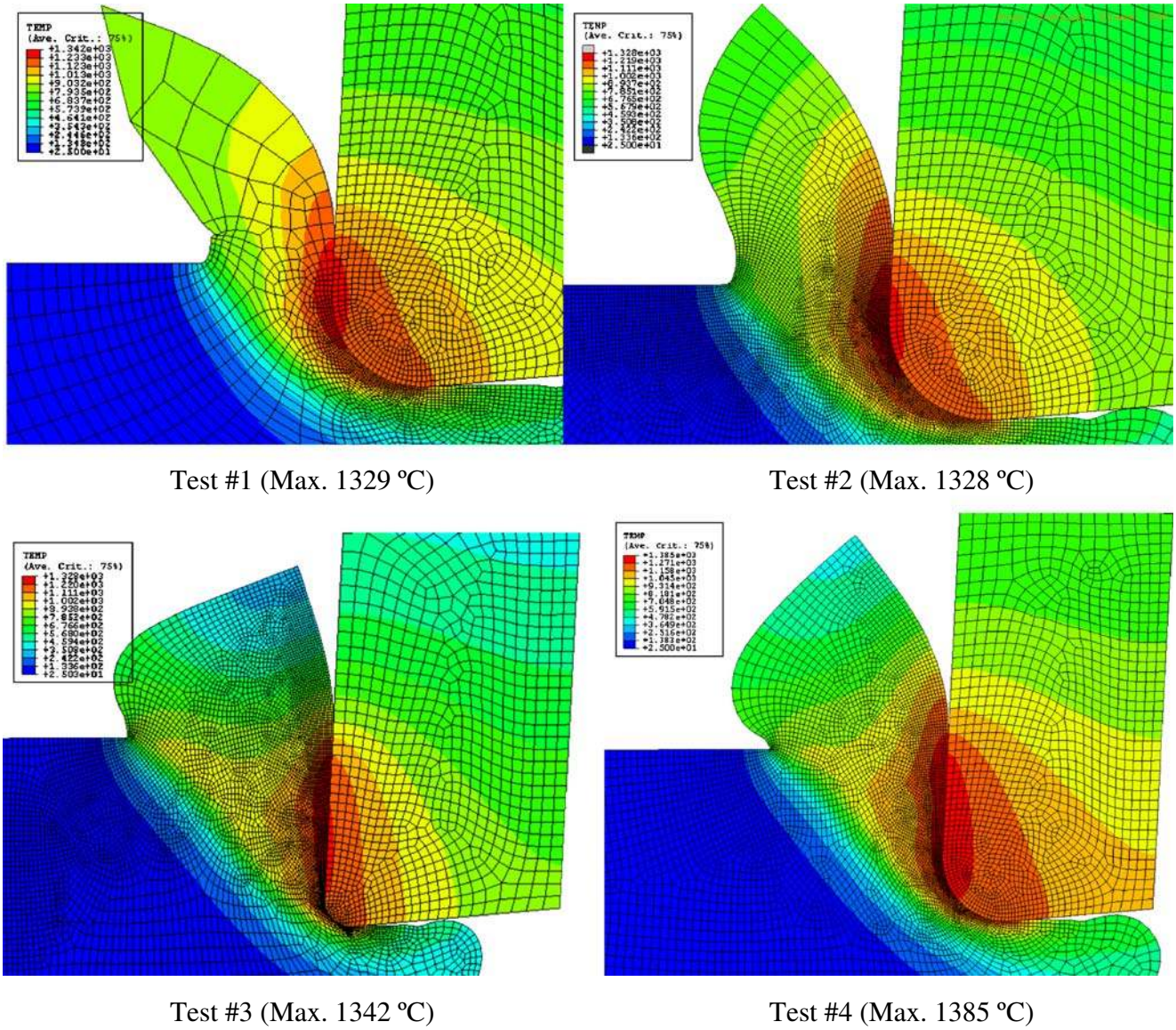

Fig. 5 Comparison of predicted temperature fields in four different test conditions

temperature fields, as discussed earlier. Therefore, fully coupled thermal-stress analysis is required for accurate predictions in FEM simulations.

In summary, the explicit dynamic method is used mainly because it has the advantages of computational efficiency for large deformation and highly non-linear problems, such as that experienced in machining. Machining, as a coupled thermal-mechanical process, could generate heat to cause thermal effects that influence mechanical effects strongly. In the mean time, work material properties change significantly as the strain rate and temperature changes. Thus, the fully coupled thermal-stress analysis, in which the temperature solution and stress solution are also carried out concurrently, is applied.

4 Simulation results and discussions

Two-dimensional FEM simulations were conducted for tests 1–4 under orthogonal machining conditions by utilizing the proposed ALE with pure Lagrangian boundaries scheme and the chip formation process from incipient to the steady state was fully observed without implementing a chip–work separation criterion. The workpiece dimensions are 1,000 μm in width and 350 μm in height. Each FEM simulation is conducted at three consecutive steps: (1) cutting, (2) tool unloading, and (3) radiation to ambient. The first step includes the chip formation stage from incipient to steady state; unlike ALE with Lagrangian and Eulerian boundaries, all of the boundaries are free and,

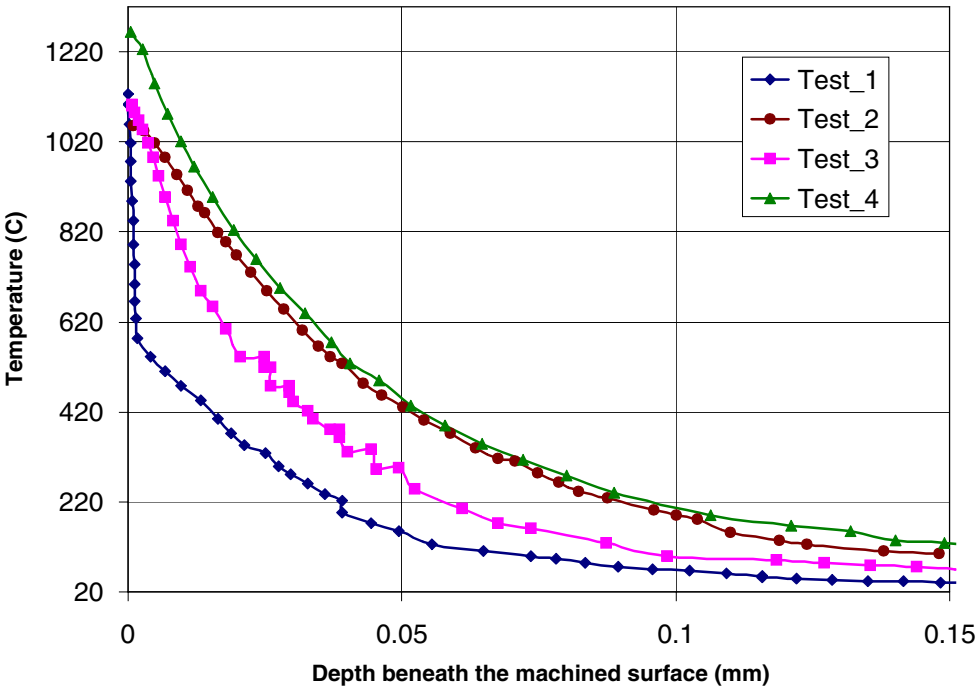

Fig. 6 Temperature distribution on the subsurface of the machined layer

therefore, a full-grown chip can be observed. The second step involves retracting the tool from the workpiece so that in-situ process conditions can be computed where the tool is fully unloaded. The third and last steps are the cooling of the workpiece by allowing radiation to the ambient. A natural stress-relief process has been observed which brings the machined surface to a state that is the closest possible to predicting realistic residual stresses fields in the workpiece. The FEM simulations have usually taken about 12 hours on a workstation equipped with an Intel Pentium 4 processor. It should be noted that the use of dual and faster processors might significantly reduce the computation time. Mesh connectivity without remeshing can be maintained for a substantial cutting length if the mesh density is increased accordingly.

4.1 Influence of edge roundness on temperature fields

The heat generated at the secondary deformation zone and at the tool–chip interface is conducted to the cutting tool and radiation to the ambient is also allowed during the cutting step. Temperature fields that have been obtained at the tool advances of 0.05 mm and 0.25 mm, during the tool unloading and cooling steps, respectively, are shown in Figs. 3 and 4, respectively. Temperature rises in the primary and secondary deformation zones are high and reach a steady state very rapidly. The maximum temperatures of 1,106°C, 1,315°C, 1,222°C, and 824°C are predicted, respectively, for the process steps under the cutting conditions of test 2, as given in Fig. 3. Similarly, the maximum temperatures of 954°C, 1,385°C, 1,350°C, and 1,285°C are predicted, respectively, for the process steps under the cutting conditions of test 4, as given in Fig. 4. However, the maximum temperatures are only effective on a concentrated spot at the tool–chip interface, whereas the temperature fields indicate a temperature distribution around the cutting zone.

Temperature fields for the machining of AISI 4340 steel at four different test conditions are presented in Fig. 5. The maximum predicted temperatures were 9.8% higher for the tool with 0.025-mm edge radius and 4.3% higher for the tool with 0.075-mm edge radius when the depth of cut increased from 0.1 mm to 0.2 mm. The maximum predicted temperature was about the same at the depth of cut of 0.1 mm, but it was 3.2% higher when the tool edge radius is increased from 0.025 mm to 0.075 mm at the 0.2-mm depth of cut. Hence, higher temperatures are predicted for cutting at greater depths of cut and with larger edge radius tools.

It is highly noticeable that the maximum temperatures occur on the tool rake face in the machining of AISI 4340 steel. Temperature distributions on the subsurface of the machined layer are also predicted as shown in Fig. 6. Higher temperatures are observed in tests 2 and 4, where the 0.075-mm edge radius tool is used. The lowest temperature profile is seen at test 1 conditions, where a lower depth of cut and smaller edge radius are provided.

4.2 Influence of edge roundness on stress fields

The fields of the predicted von Mises stress components, σ_{11} and σ_{33}, also represent the machining-induced stresses on the subsurface of the workpiece, as given in the Fig. 7.

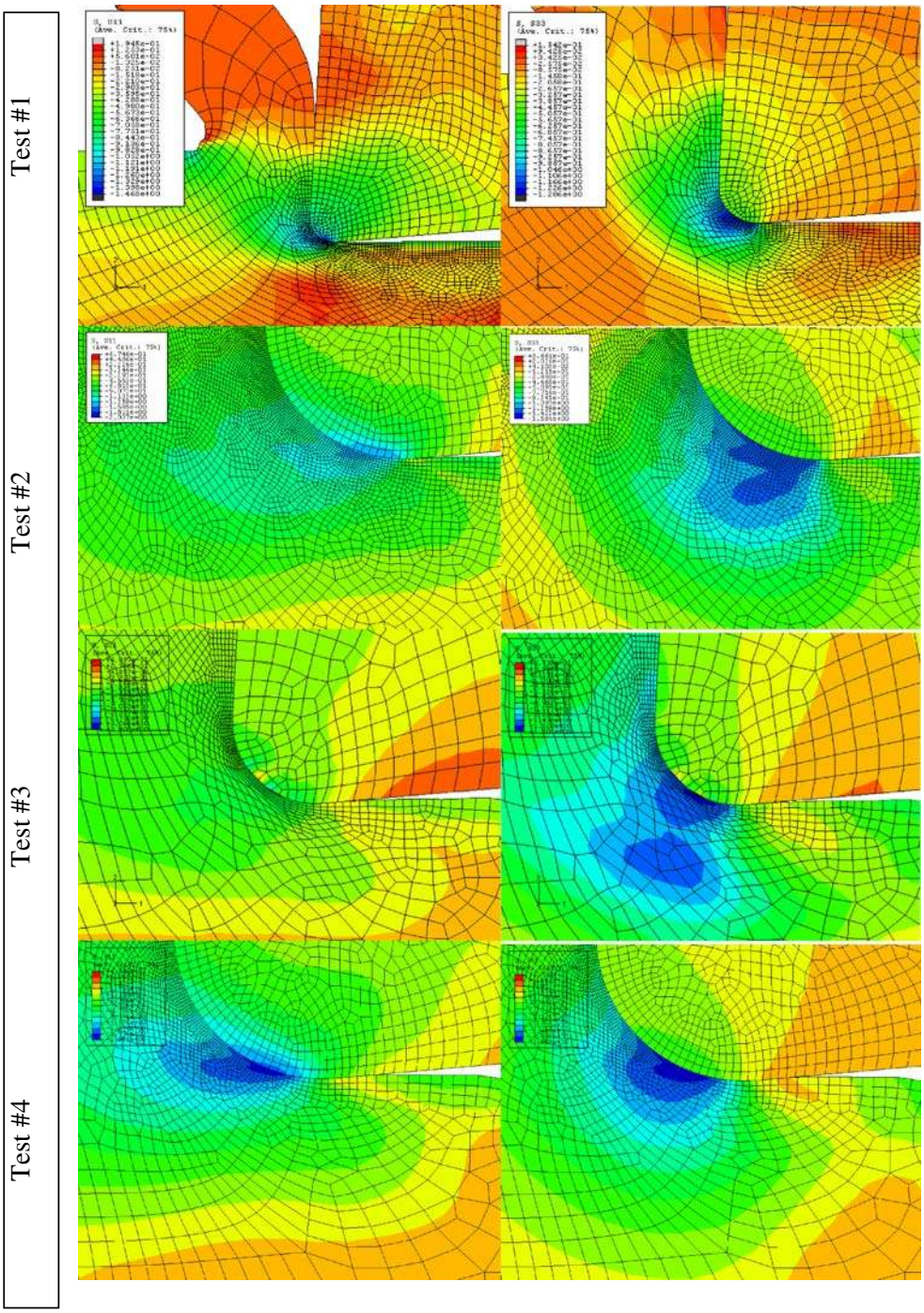

Fig. 7 Comparison of predicted stress fields of σ_{11} and σ_{33} in four different test conditions

From the simulation results, it was observed that there exists a region of very high deformation rate around the round edge of the cutting tool. As the tool edge roundness increases, the machining-induced residual stresses also increase. Hence, the round edge of the cutting tool and the highly deformed region underneath has a dominant influence on the residual stresses of the machined surface. This also signifies the proposed work when compared to the earlier FEM modeling studies that relied on chip–workpiece separation criteria. The use of a separation criterion undermines the effect of the cutting edge on the residual stress formation on the machined surface. In this study, the work material is allowed to flow around the round edge of the cutting tool and, therefore, the physical process has been simulated more realistically.

Machining-induced residual stress profiles with respect to the depth beneath the machined surface for von Mises stresses, stress components σ_{11} and σ_{33}, are also computed from the simulated stress fields. A path prescribed underneath the round edge of the tool is tracked for obtaining the

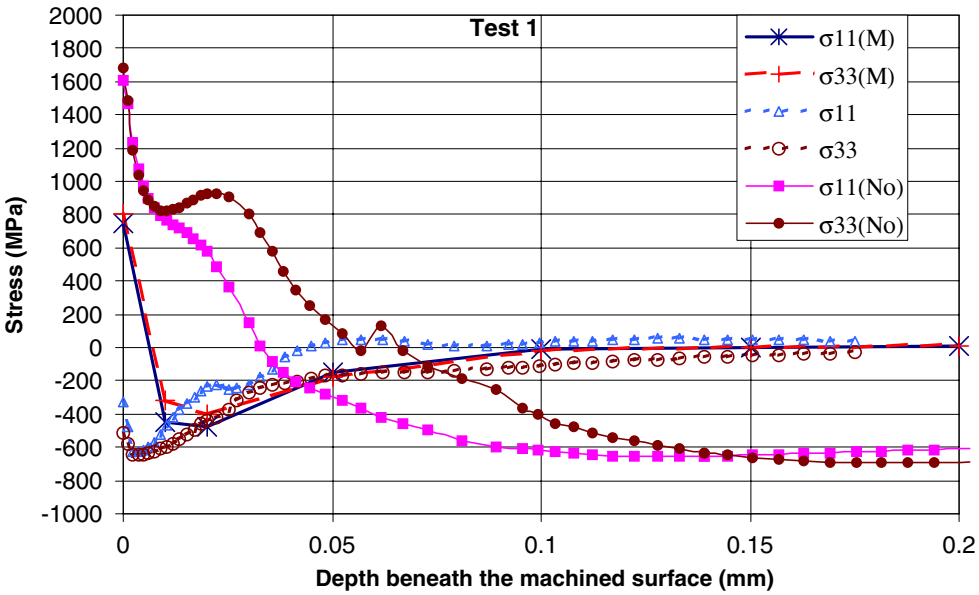

Fig. 8 Comparison of the predicted and measured (Jacobus et al. [33]) stress fields in the orthogonal cutting of AISI 4340 steel (test 1: edge radius=0.025 mm, t_u=0.1 mm, V=300 m/min)

stress components with respect to the depth inside the machined surface utilized in each FEM simulation. Machining-induced stresses are predicted along those paths that are presented in Figs. 8, 9, 10, and 11, as compared with the experimentally measured machining-induced residual stresses presented by Jacobus et al. [33]. In these figures, the stress components; σ_{11} (M) and σ_{33} (M), σ_{11} and σ_{33}, and σ_{11} (No) and σ_{33} (No) represent the measured, predicted while tool is in contact, and predicted when tool makes no contact with the workpiece, respectively. As can be seen from the Figs. 8, 9, 10, and 11, the predicted subsurface stress components were highly compressive; however, as the tool unloaded and the workpiece was cooled and stress relieved, the residual stresses become more tensile than compressive. The larger edge radius produced larger compressive stresses on the subsurface and the increased depth of cut slightly reduced the compressive stresses.

The machining-induced state of stress is the highest in tests 1 and 3. However, the von Misses stress is significantly lower on the machined layer in the machining of AISI 4340 steel when machining with larger edge radius cutting tools, indicating the significant influence of the edge roundness on the machining-induced stresses.

In test 1, as shown in Fig. 8, where a radius of 0.025 mm tool edge was used, the predicted stresses while the tool is in contact with the workpiece were found to be closer to the measured stresses. When the tool is unloaded and the workpiece is cooled and the stress relieved, the stresses

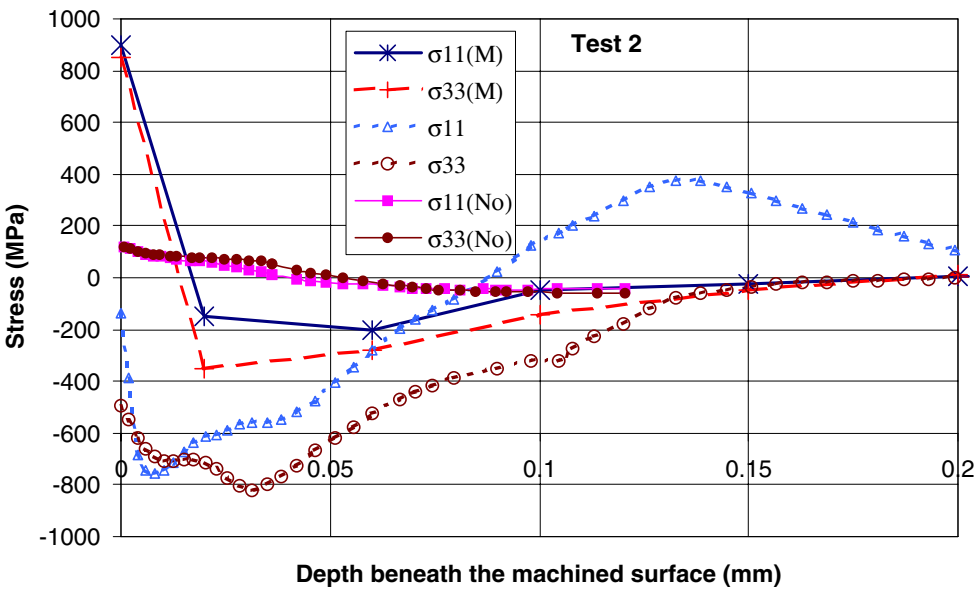

Fig. 9 Comparison of the predicted and measured (Jacobus et al. [33]) stress fields in the orthogonal cutting of AISI 4340 steel (test 2: edge radius=0.075 mm, t_u=0.1 mm, V=300 m/min)

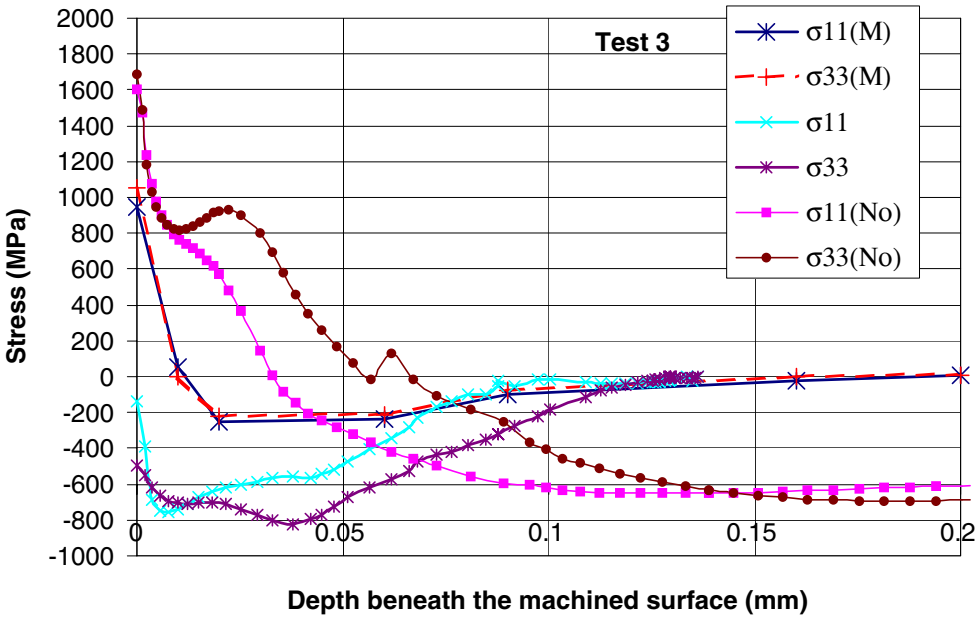

Fig. 10 Comparison of the predicted and measured (Jacobus et al. [33]) stress fields in the orthogonal cutting of AISI 4340 steel (test 3: edge radius=0.025 mm, t_u=0.2 mm, V=300 m/min)

beneath the machined surface were found to be mostly tensile near the surface, but largely compressive at depths greater than 0.05 mm.

In test 2, as shown in Fig. 9, where a radius of 0.075 mm tool edge was used, the predicted stresses were largely compressive on the subsurface, but the σ_{11} component was found to be tensile for the depth between 0.1 mm and 0.2 mm. This indicates that larger edge radius tools affect the residual stress profile to a greater depth and may result in tensile subsurface stresses. In these test conditions, when the tool is unloaded and the workpiece is released, the residual stress fields were found to be slightly tensile.

Similar behavior has been observed in tests 3 and 4, as shown in Figs. 10 and 11, respectively, where a larger depth of cut (0.2 mm) was taken. The increased depth of cut results in slightly larger residual stresses on the machined surface and the subsurface.

In summary, these stress field predictions can be combined with the temperature field predictions and can be fed into surface property models that are highly essential to further predict surface integrity and thermo-mechanical deformation related property alteration on the microstructure of the machined surfaces. Today, most of the surface property models are empirical and are still not sufficient for determining the full surface morphology induced by machining, especially finish machining, where most of the machining is done with the edge geometry of the cutting tool.

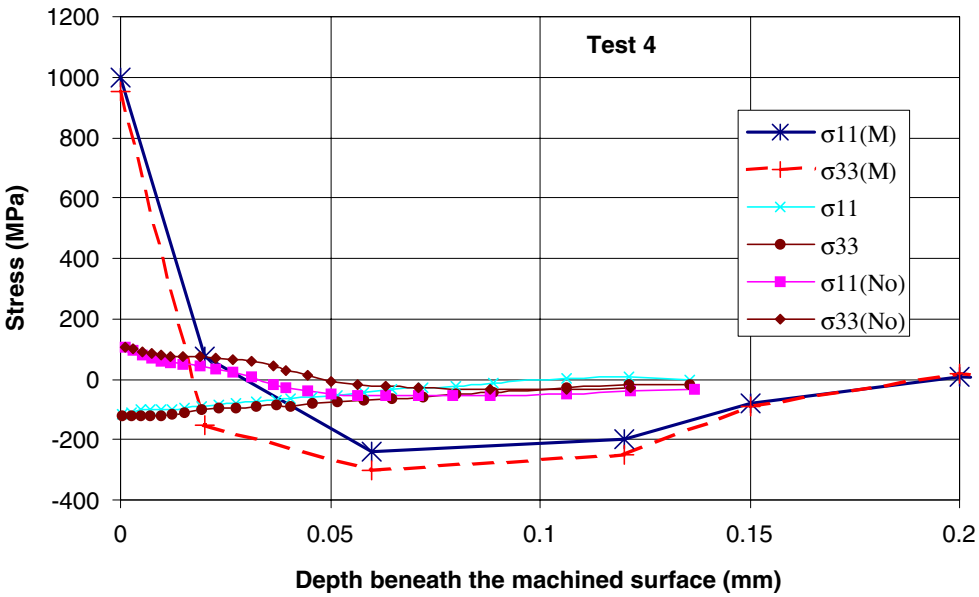

Fig. 11 Comparison of the predicted and measured (Jacobus et al. [33]) stress fields in the orthogonal cutting of AISI 4340 steel (test 4: edge radius=0.075 mm, t_u=0.2 mm, V=300 m/min)

5 Conclusions

In this study, we have utilized the explicit dynamic arbitrary Lagrangian Eulerian (ALE) method with adaptive meshing capability and developed a finite element model (FEM) simulation model for the orthogonal cutting of AISI 4340 steel using round edge carbide cutting tools without employing a remeshing scheme and without using a chip separation criterion. The extended Johnson-Cook work material model and a detailed friction model are also employed and the work material flow around the round edge of the cutting tool is simulated in conjunction with an adaptive meshing scheme. The development of temperature fields during the cutting process is also captured. Very high and localized temperatures are predicted at the tool–chip interface due to a detailed friction model. Predictions of the von Mises stress fields in the chip, in the tool, and on the machined surface are effectively carried out. Process-induced stress profiles depict that there exist both compressive and tensile stress regions beneath the surface. FEM modeling of the stresses and resultant surface properties induced by round edge cutting tools is performed for the high-speed machining (HMS) of AISI 4340 steel. After the FEM simulations are complete for different edge radii and depths of cut, the tool is unloaded and the stresses are relieved. The predicted stress fields are compared with experimentally measured residual stresses obtained from the literature. The results indicate that the round edge design tools influence the stress and temperature fields greatly. These predictions combined with the temperature field predictions are highly essential to further predict surface integrity and thermo-mechanical deformation related property alteration on the microstructure of the machined surfaces. It has been demonstrated that the ALE simulation approach presented in this work, without remeshing and without using a chip separation criterion, results in better predictions for machining-induced stresses.

Acknowledgments The authors acknowledge the support provided by Rutgers University Research Council grants and ABAQUS Inc. for the use of software licenses.

References

1. Usui E, Shirakashi T (1982) Mechanics of machining—from descriptive to predictive theory. In on the art of cutting metals—75 years later. ASME Pub PED 7:13–35
2. Komvopoulos K, Erpenbeck SA (1991) Finite element modeling of orthogonal metal cutting. ASME J Eng Ind 113(3):253–267
3. Lin ZC, Lin SY (1992) A coupled finite element model of thermo-elastic-plastic large deformation for orthogonal cutting. ASME J Eng Ind 114:218–226
4. Zhang B, Bagchi A (1994) Finite element simulation of chip formation and comparison with machining experiment. ASME J Eng Ind 116(8):289–297
5. Shih AJ (1995) Finite element simulation of orthogonal metal cutting. ASME J Eng Ind 117:84–93
6. Strenkowski JS, Carroll JT (1985) A finite element model of orthogonal metal cutting. ASME J Eng Ind 107:346–354
7. Strenkowski JS, Carroll JT (1986) Finite element models of orthogonal cutting with application to single point diamond turning. Int J Mech Sci 30(12):899–920
8. Black JT, Huang JM (1996) An evaluation of chip separation criteria for the FEM simulation of machining. ASME J Manuf Sci Eng 118 545–553
9. Sekhon GS, Chenot JL (1992) Some simulation experiments in orthogonal cutting. Numerical Methods Industrial Forming Process 901–906
10. Marusich TD, Ortiz M (1995) Modeling and simulation of high-speed machining. Int J Numer Methods Eng 38:3675–3694
11. Ceretti E, Fallböhmer P, Wu WT, Altan T (1996) Application of 2-D FEM to chip formation in orthogonal cutting. J Mate Process Technol 59(1–2):169–181
12. Leopold J, Semmler U, Hoyer K (1999) Applicability, robustness and stability of the finite element analysis in metal cutting operations. In: Proceedings of the 2nd CIRP International Workshop on Modeling of Machining Operations, Nantes, France, January 1999, pp 81–94
13. Özel T, Altan T (2000) Determination of workpiece flow stress and friction at the chip–tool contact for high-speed cutting. Int J Mach Tools Manuf 40(1):133–152
14. Madhavan V, Chandrasekar S, Farris TN (2000) Machining as a wedge indentation. J Appl Mech 67(1):128–139
15. Klocke F, Raedt H-W, Hoppe S (2001) 2D-FEM simulation of the orthogonal high speed cutting process. Machi Sci Technol 5 (3):323–340
16. Baker M, Rosler J, Siemers C (2002) A finite element model of high speed metal cutting with adiabatic shearing. Comput Struct 80:495–513
17. Rakotomalala R, Joyot P, Touratier M (1993) Arbitrary Lagrangian-Eulerian thermomechanical finite element model of material cutting. Commun Numer Methods Eng 9(12):975–987
18. Olovsson L, Nilsson L Simonsson, K (1999) An ALE formulation for the solution of two-dimensional metal cutting problems. Comput Struct 72(4–5):497–507
19. Movahhedy MR, Gadala MS, Altintas Y (2000) FE modeling of chip formation in orthogonal metal cutting process: an ALE approach. Mach Sci Technol 4:15–47
20. Movahhedy MR, Altintas Y, Gadala MS (2002) Numerical analysis of metal cutting with chamfered and blunt tools. ASME J Manuf Sci Eng 124(2):178–188
21. Adibi-Sedeh AH, Madhavan V (2003) Understanding of finite element analysis results under the framework of Oxley's machining model. In: Proceedings of the 6th CIRP International Workshop on Modeling of Machining Operations, Hamilton, Canada, May 2003
22. Haglund AJ, Kishawy HA, Rogers RJ On friction modeling in orthogonal machining: an arbitrary Lagrangian-Eulerian finite element model. Trans NAMRI/SME 33:589–596
23. Özel T, Zeren E (2005) Finite element method simulation of machining of AISI 1045 steel with a round edge cutting tool. In: Proceedings of the 8th CIRP International Workshop on Modeling of Machining Operations, Chemnitz, Germany, May 2005, pp 533–542
24. Özel T (2003) Modeling of hard part machining: effect of insert edge preparation for CBN cutting tools. J Mater Process Technol 141:284–293
25. Yen Y-C, Jain A, Altan T (2004) A finite element analysis of orthogonal machining using different toll edge geometries. J Mater Process Technol 146(1):72–81
26. Chuzhoy L, DeVor RE, Kapoor SG (2003) Machining simulation of ductile iron and its constituents. Part 2: numerical simulation

and experimental validation of machining. ASME J Manuf Sci Eng 125(2):192–201
27. Yang X, Liu CR (2002) A new stress-based model of friction behavior in machining and its significant impact on residual stresses computed by finite element method. Int J Mech Sci 44(4):703–723
28. Liu CR, Guo YB (2000) Finite element analysis of the effect of sequential cuts and tool–chip friction on residual stresses in a machined layer. Int J Mech Sci 42(6):1069–1086
29. Guo YB, Liu CR (2002) 3D FEA modeling of hard turning. ASME J Manuf Sci Eng 124(2):189–199
30. Guo YB, Wen Q (2005) A hybrid modeling approach to investigate chip morphology transition with the stagnation effect by cutting edge geometry. Trans NAMRI/SME 33:469–476
31. Davies MA, Cao Q, Cooke AL, Ivester R (2003) On the measurement and prediction of temperature fields in machining of AISI 1045 steel. Annals CIRP 52(1):77–80
32. Deshayes L, Ivester R, Mabrrouki T, Rigal J-F (2004) Serrated chip morphology and comparison with finite element simulations. In: Proceedings of the 2004 International Mechanical Engineering Congress (IMECE 2004), Anaheim, California, November 2004
33. Jacobus K, DeVor RE, Kapoor SG (2000) Machining-induced residual stress: experimentation and modeling. ASME J Manuf Sci Eng 122(1):20–31
34. Johnson GR, Cook WH (1983) A constitutive model and data for metals subjected to large strains, high strain rates and high temperatures. In: Proceedings of the 7th International Symposium on Ballistics, The Hague, The Netherlands, April 1983, pp 541–547
35. Ng E-G, El-Wardany TI, Dumitrescu M, Elbastawi MA (2002) Physics-based simulation of high speed machining. Mach Sci Technol 6(3):301–329
36. Özel T, Zeren E (2006) A methodology to determine work material flow stress and tool–chip interfacial friction properties by using analysis of machining. ASME J Manuf Sci Eng 128 (1):119–129
37. Özel T, Zeren E (2005) Finite element modeling of stresses induced by high speed machining with round edge cutting tools. In: Proceedings of the 2005 International Mechanical Engineering Congress (IMECE 2005), Orlando, Florida, November 2005, paper no. 81046